Received: 11 May 2021 | Revised: 31 August 2021 | Accepted: 17 September 2021

DOI: 10.1002/ese3.989

ORIGINAL ARTICLE

Energy Science & Engineering Open Access

A modified pulse-decay approach to simultaneously measure permeability and porosity of tight rocks

Yue Wang[1] | **Steffen Nolte**[2] | **Zhiguo Tian**[1] | **Alexandra Amann-Hildenbrand**[2] | **Bernhard Krooss**[2] | **Moran Wang**[1]

[1]Department of Engineering Mechanics, Tsinghua University, Beijing, China

[2]Institute of Geology and Geochemistry of Petroleum and Coal, Energy and Mineral Resources Group (EMR), RWTH Aachen University, Aachen, Germany

Correspondence
Moran Wang, Department of Engineering Mechanics, Tsinghua University, Beijing 100084, China.
Email: mrwang@tsinghua.edu.cn

Funding information
National Natural Science Foundation of China, Grant/Award Number: U1837602 and 11761131012; Tsinghua University Initiative Scientific Research Program

Abstract

Permeability and porosity are the two most important parameters of rocks for the evaluation and exploitation of oil/gas reservoirs. In this study, a modified pulse-decay method has been developed to measure both permeability and porosity simultaneously. In the present method, the gas pressure in one chamber is changed (increased or decreased) instantaneously and then maintained constant, while the pressure response changing with time in the other one is monitored. A mathematical model of this procedure has been formulated, and a general analytical solution, including the early-time and late-time evolutions, has been obtained. The late-time solution is presented for postprocessing of experimental data, which leads to the simultaneous measurement of permeability and porosity values of tight rocks. Our measurements agree well with those from the classical pulse-decay and gas expansion methods. Compared with measuring the permeability and porosity separately, the proposed method can reduce the total test time and ensure the permeability and porosity are measured under the same effective stress condition.

KEYWORDS

permeability, porosity, porous media, pulse-decay method, tight rocks

1 | INTRODUCTION

The study of unconventional reservoirs continues to attract increasing attention around the world due to their tremendous potential for future gas reserves and production.[1-5] Permeability characterizes the fluid flow rate through the rock formation under the pressure gradient and therefore is one of the most important parameters for the evaluation and exploitation of unconventional reservoirs. Compared with conventional reservoirs, unconventional reservoirs usually have extremely low permeability, which brings difficulty to permeability measurement.[6-8]

Many methods have been developed to determine rock permeability in the laboratory and can be subdivided into two kinds based on their steady-state or unsteady-state nature.[9,10] The steady-state methods measure the steady-state flow rate under a given pressure gradient, and the unsteady-state methods measure transient pressure variations. Generally, the unsteady-state methods are more suitable for measurements on tight rocks than the steady-state methods, because the pressure is easier to measure than the flow rate across tight rock samples, which is often too small to be detected.[11,12]

The pulse-decay method is one of the most widely used unsteady-state methods.[13,14] The basic idea was pioneered by Brace et al.[15] In the conventional pulse-decay measurement, a sample is placed in the core holder and two chambers are connected to its two ends. Initially, the whole system is in pressure equilibrium and then a pressure pulse is applied to one chamber. The pressure variations with time in both chambers are recorded. Unlike the steady-state method, where the permeability can be calculated directly with Darcy's law, the pulse-decay method requires an analytical solution to evaluate the permeability from the pressure record. Brace et al.[15] obtained an approximate analytical solution by assuming a constant pressure gradient within the core, which is valid when the pore volume of the sample is negligible compared with the chambers. Hsieh et al.[16] and Dicker and Smits[17] gave a general solution without the assumption used by Brace et al.[15] The analytical solution with considerations for gas adsorption was developed by Cui et al.[18] Yang et al.[19] gave the solution for the transverse permeability measurements on tight core samples. Han et al.[20] summarized the analytical solutions of pulse-decay methods and compared their performance under different scenarios.

In recent decades, many modified pulse-decay methods with different experimental designs have also been developed. Giot et al.[21] suggested measuring the permeability by imposing a pressure pulse on a hollow cylindrical sample, and similar ideas have also been proposed by other researchers.[22,23] Yang et al.[24] presented a method in which one side of the sample was connected to the chamber and the other side was sealed. The radial differential pressure decay method was developed by Wu et al.[10] to assess the apparent permeability with microplug samples. Metwally and Sondergeld[25] proposed the pressure build-up method where the upstream pressure was kept constant during the test and the downstream pressure increase was recorded for permeability evaluation. Further research[26] showed the pressure build-up method is less affected by surface defects or limited penetration fractures of the core plugs than the conventional pulse-decay method because the downstream pressure build-up is a response across the whole core plug, unlike the conventional pulse-decay response.

Despite the wide range of usage and the potential advantages, the original pressure build-up method suffers from the separation of permeability and porosity measurements. In the pulse-decay methods where chambers of finite volume are used, the porosity can be evaluated by mass conservation and Boyle's law using the initial and final equilibrium pressure.[7,27,28] However, the total mass in the pressure build-up method is not conserved because

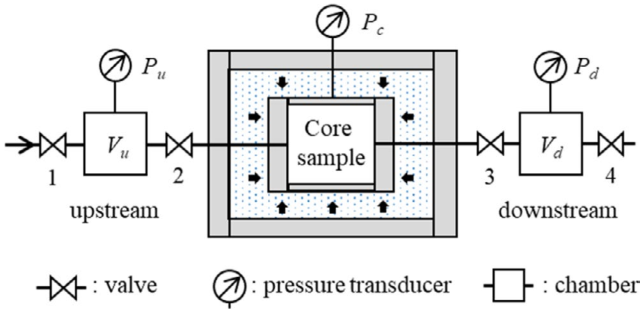

FIGURE 1 The schematic of the experimental setup

the pressure on one side is kept constant during the test, which brings difficulty to porosity measurement in the pressure build-up method.

To overcome this problem, this study proposes a modified method that can simultaneously measure the permeability and the porosity in a single test. In this method, the pressure in the downstream (or upstream) chamber is decreased (or increased) and then maintained constant. The pressure variations in the other chamber are used to evaluate the permeability and porosity of the tight rock sample. The mathematical model and the analytical solution based on this experimental design have been obtained. Using the proposed method, the permeability and the porosity of a tight sandstone sample have been measured and the accuracy of the results has been confirmed.

2 | EXPERIMENTAL PROCEDURE

The schematic of the experimental setup is shown in Figure 1. A detailed description of the experimental setup can be found in our previous studies.[29,30] Since applying a negative pulse in the downstream chamber and applying a positive pulse in the upstream chamber are mathematically equivalent, we only take the former as an example in the following part of the study. To keep the downstream pressure constant during the test, the downstream volume is chosen to be much larger than the sum of the pore volume and the volume of the upstream chamber, that is, $V_d \gg V_p + V_u$, or to be open to the atmosphere. The experimental protocol is as follows:

1. The core sample was placed into the core holder and confining pressure was applied to resemble the subsurface condition. An oven was used to keep the whole setup at the desired temperature.
2. With valves 1, 2, 3 open, and valve 4 closed, the core and the two chambers were filled to the desired initial pressure. Then, valves 1, 2, and 3 were closed, and valve 4 was open. The pressure in the downstream chamber was decreased to create the initial pressure difference (<10%) and then maintained as constant.

3. Valve 4 was closed and then valves 2, 3 were open. The pressure decay in the upstream chamber was recorded with the transducer.

Figure 2 shows the schematic of the pressure profile within the system at different instants. The characteristic of the proposed method is that the pressure in the downstream, where the pulse is applied and the Joule-Thomson effect occurs, is kept constant, and the pressure in the upstream, where there is no pulse, is recorded to evaluate the petro-physical properties of the sample. This design helps to eliminate the influence of the Joule-Thomson effect on the pressure recording.

3 | MATHEMATICAL DERIVATION

3.1 | The governing equation

By combining the law of mass conservation and Darcy's law,[15-17] the gas flow within the sample during the pulse-decay process can be described by a one-dimensional diffusion equation as:

$$\frac{\partial P}{\partial t} = \frac{k}{\beta\mu\phi}\frac{\partial^2 P}{\partial x^2} \tag{1}$$

where P is the gas/pore pressure (Pa), k the permeability coefficient (m^2), β the gas compressibility (Pa^{-1}), μ the gas dynamics viscosity (Pa·s), and ϕ is the sample porosity. Strictly speaking, k, β, μ and ϕ are all pressure-dependent. For example, the gas compressibility β is related to pressure

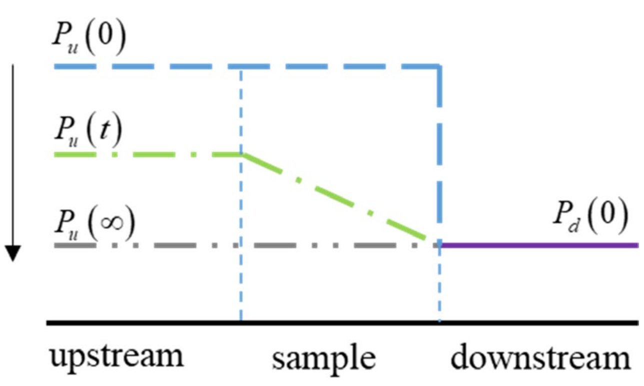

FIGURE 2 The schematic of the pressure profile variations. During the test, the downstream pressure is kept at $P_d(0)$. At $t = 0$, the sample and the upstream are in pressure equilibrium at $P_u(0) > P_d(0)$. When $t > 0$, the gas flows from the upstream through the sample to the downstream, and the upstream pressure $P_u(t)$ decreases until it equals the downstream pressure, that is, $P_u(\infty) = P_d(0)$

through the equation of state, and the permeability coefficient k is affected by pressure due to the poroelastic and slippage effects.[31-33] However, as previously noted,[15,34-36] when the initial pressure difference between the two ends of the sample in a single measurement is small, these variables can be regarded as constants and their values are taken under the mean pore pressure.

Considering the mass balance at the interface between the core sample and the upstream chamber and noting that the downstream pressure is kept constant during the test, the boundary conditions are obtained:

$$\left.\frac{\partial P}{\partial t}\right|_{x=0} = \frac{kA}{\beta\mu V_u}\left.\frac{\partial P}{\partial x}\right|_{x=0}, \quad \left.\frac{\partial P}{\partial t}\right|_{x=L} = 0 \tag{2}$$

where A is the cross-section area of the sample (m^2), V_u the upstream chamber volume (m^3), and L is the length of the sample (m).

The initial conditions are as follows:

$$P(x,0) = \begin{cases} P_u(0), & 0 \le x < L \\ P_d(0), & x = L \end{cases} \tag{3}$$

where $P_u(0)$ and $P_d(0)$ are the initial upstream and downstream pressures (Pa), respectively.

To facilitate the derivation, the following dimensionless variables with subscript D are introduced:

$$x_D = \frac{x}{L}, t_D = \frac{kt}{\beta\mu\phi L^2}, P_D = \frac{P(x,t) - P_d(0)}{P_u(0) - P_d(0)}, a = \frac{LA\phi}{V_u} \tag{4}$$

With these dimensionless variables, the governing Equation (1) can be rewritten as:

$$\frac{\partial P_D}{\partial t_D} = \frac{\partial^2 P_D}{\partial x_D^2} \tag{5}$$

The dimensionless boundary conditions are given by:

$$\left.\frac{\partial P_D}{\partial t_D}\right|_{x_D=0} = a\left.\frac{\partial P_D}{\partial x_D}\right|_{x_D=0}, \quad \left.\frac{\partial P_D}{\partial t_D}\right|_{x_D=1} = 0 \tag{6}$$

and the dimensionless initial conditions are as follows:

$$P_D(x_D,0) = \begin{cases} 1, & 0 \le x_D < 1 \\ 0, & x_D = 1 \end{cases} \tag{7}$$

3.2 | The analytical solution

The Laplace transform is used to solve the above equations (the details can be found in the appendixes), and the derived solutions are shown below.

3.2.1 | The general solution

The general solution for the dimensionless pressure distribution within the sample is:

$$P_D\left(x_D, t_D\right) = 2\sum_{m=1}^{\infty} \frac{a\cos\left(\theta_m x_D\right) - \theta_m \sin\left(\theta_m x_D\right)}{\left(\theta_m^2 + a^2 + a\right)\cos\left(\theta_m\right)} e^{-\theta_m^2 t_D} \quad (8)$$

where θ_m is the mth positive root of:

$$\tan\theta_m = \frac{a}{\theta_m} \quad (9)$$

The general solutions for upstream and downstream pressures can be obtained by setting $x_D = 0$ and $x_D = 1$ in Equation (8), respectively:

$$P_{uD}\left(t_D\right) = P_D\left(0, t_D\right) = \sum_{m=1}^{\infty} \frac{2a}{\left(\theta_m^2 + a^2 + a\right)\cos\theta_m} e^{-\theta_m^2 t_D} \quad (10)$$

$$P_{dD}\left(t_D\right) = P_D\left(1, t_D\right) = 0 \quad (11)$$

The expression for dimensionless pressure difference between two ends of the sample is given by:

$$\Delta P_D\left(t_D\right) = P_{uD}\left(t_D\right) - P_{dD}\left(t_D\right) = \sum_{m=1}^{\infty} \frac{2a}{\left(\theta_m^2 + a^2 + a\right)\cos\theta_m} e^{-\theta_m^2 t_D} \quad (12)$$

The pressure distributions throughout the sample at different instants are depicted in Figure 3. Because the negative pulse needs time to permeate through the core sample from the downstream to the upstream, the upstream pressure remains constant rather than lowering immediately after the test begins. As time proceeds, the domain affected by the negative pulse expands and eventually reaches the upstream side of the core, after which a significant decrease in the upstream pressure can be observed.

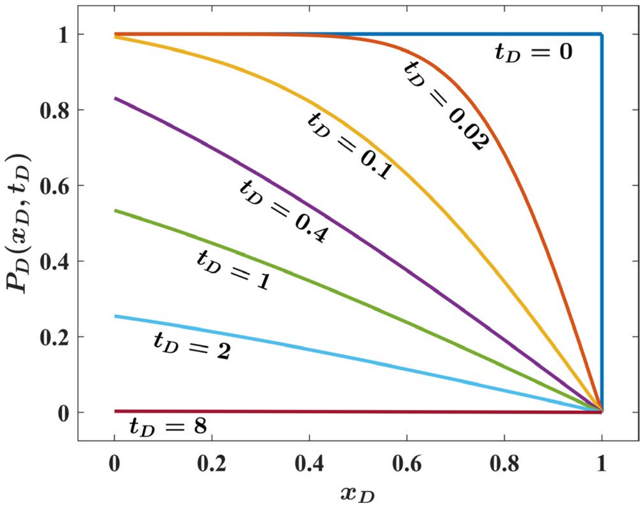

FIGURE 3 Pressure distributions within the sample as time proceeds ($a = 1$)

3.2.2 | The early-time solution

The approximate solution that describes the upstream pressure variations at the beginning of the pulse-decay test is usually referred to as the early-time solution in the literature.[9,16,19] The early-time solution to the proposed method is:

$$P_{uD}\left(t_D\right) \approx 1 + 2e^{a + a^2 t_D}\operatorname{erfc}\left(a\sqrt{t_D} + \frac{1}{2\sqrt{t_D}}\right) - 2\operatorname{erfc}\left(\frac{1}{2\sqrt{t_D}}\right) \quad (13)$$

where erfc denotes the complementary error function.

As shown in Figure 4, when the dimensionless time t_D is small, the early-time solution (13) approximates the general solution (10) very well. However, due to the complication of the complementary error function, Equation (13) is not used for permeability and porosity evaluation in this study.

3.2.3 | The late-time solution

Although the general solution for pressure difference (Equation 12) is valid at any time of the test, it is difficult to use directly, because of its form of an infinite series. As shown in Figure 5, we found that $\theta_1 < \theta_2 < \theta_3 < \cdots$. Thus, when time is large (i.e., at the late-time stage of the test), all the exponential terms with $m > 1$ decay much faster than the term with $m = 1$, and Equation (12) reduces to a single exponential form:

$$\Delta P_D\left(t_D\right) \approx \frac{2a}{\left(\theta_1^2 + a^2 + a\right)\cos\theta_1} e^{-\theta_1^2 t_D} \quad (14)$$

which is referred to as the late-time solution in the literature.[9]

The comparison between the general solution and the late-time solution for pressure difference is presented in Figure 6, and the results show that when the dimensionless

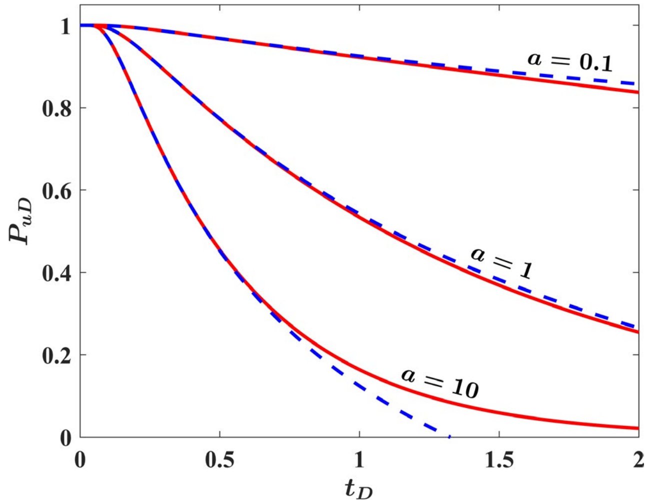

FIGURE 4 The comparison between the general solution (Equation 10, solid lines) and the early-time solution (Equation 13, dashed lines) for upstream pressure with different volume ratios

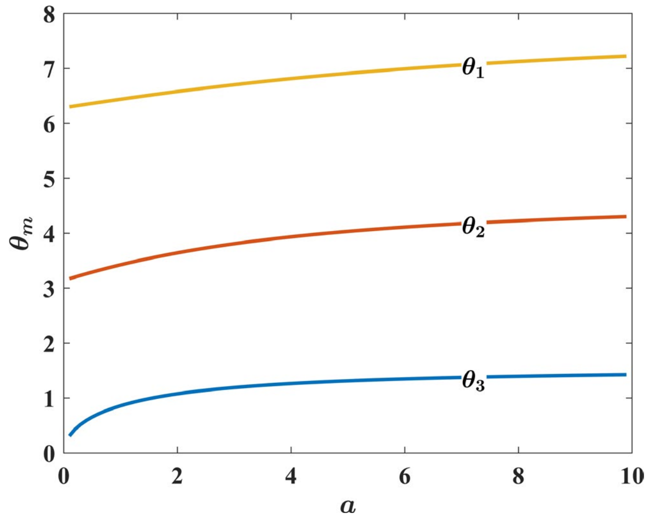

FIGURE 5 The variations of θ_m ($m = 1,\ 2,\ 3$) with volume ratio a

time t_D is large, the two solutions agree with each other very well.

3.3 | Permeability and porosity determination

Taking the logarithm of the late-time solution for pressure difference (Equation 14) yields:

$$\ln\Delta P_D = f - \theta_1^2 t_D = f + \alpha t \tag{15}$$

where the dimensionless time is transformed into the dimensional one, and the expressions for f and α are as follows:

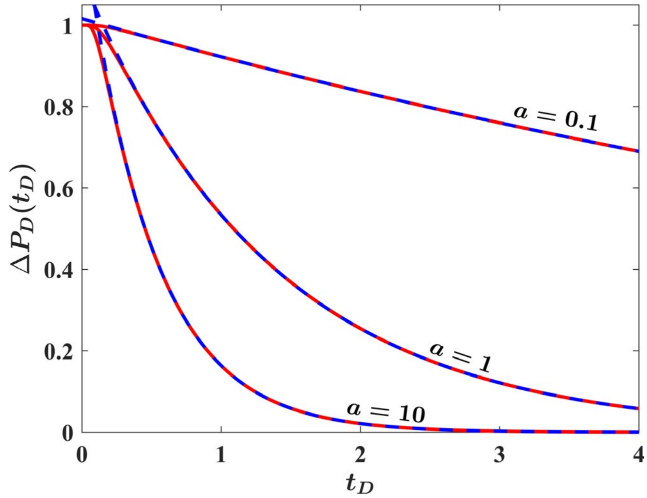

FIGURE 6 The comparison between the general solution (Equation 10, the solid lines) and the late-time solution (Equation 14, the dashed lines) for pressure difference with different volume ratios

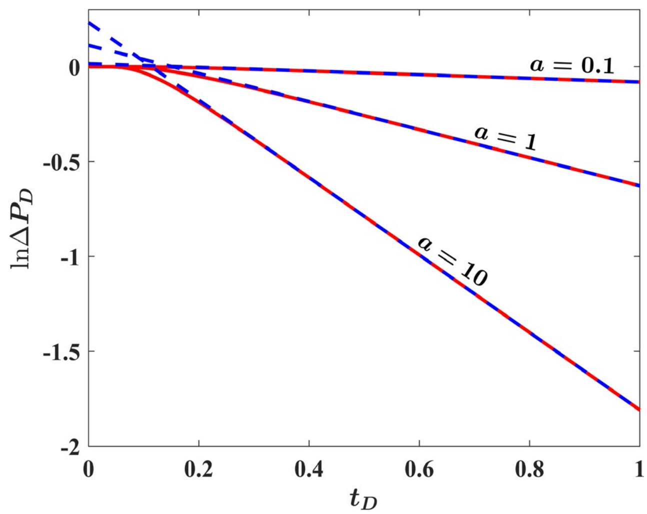

FIGURE 7 The logarithmic pressure difference vs time for different volume ratios. The solid lines represent the general solution (Equation 12) and the dashed lines represent the late-time solution (Equation 15). The x-axis here is the dimensionless time t_D, so the slope and the intercept of the late-time solution are $-\theta_1^2$ and f, respectively

$$f = \ln\frac{2a}{\left(\theta_1^2 + a^2 + a\right)\cos\theta_1} \tag{16}$$

$$\alpha = -\frac{\theta_1^2 k}{\beta\mu\phi L^2} \tag{17}$$

Equation (15) indicates that if the logarithmic dimensionless pressure difference $\ln\Delta P_D$ is plotted against t_D or t, a linear relationship can be obtained in the late-time stage, where the intercept is f, and the slope is $-\theta_1^2$ or α, respectively.

It is noted that a one-to-one correspondence between a and θ_1 can be established through Equation (9). Therefore, by combining Equations (9) and (16), f can be solely determined if a or θ_1 is known, and vice versa. Different values of a and the corresponding values of f are shown in Figures 7 and 8, from which a monotonic relationship between a and f is found. In other words, a one-to-one correspondence between the intercept f and the volume ratio a can be established, so the intercept f obtained from the experiment can be used to calculate the volume ratio a and therefore the porosity ϕ. A similar relationship can be found between the f and θ_1 (see Figures 7 and 9).

Equations (9) and (16) are both transcendental equations, so the mappings from intercept f to a and θ_1 are both implicit functions, that is, the expressions for $a(f)$ and $\theta_1(f)$ cannot be written down in an explicit manner. For ease of use, a series of values of (a,f) and $\left(\theta_1,f\right)$ are obtained by solving Equations (9) and (16) numerically, and two analytical approximate correlations are given by fitting the series of values with polynomial and rational fractions, respectively:

$$a = 3091.7f^4 - 684.46f^3 + 76.014f^2 + 4.5344f \quad (18)$$

$$\theta_1 = \left(4.123f^2 + 0.4846f + 3.484 \times 10^{-4}\right) / (f + 0.01263) \quad (19)$$

The relative error between these correlations and the exact values is smaller than 1% when $a < 3$. Equations (18) and (19) can be used to interpret the volume ratio a and θ_1 directly from the intercept f, respectively. Then, the

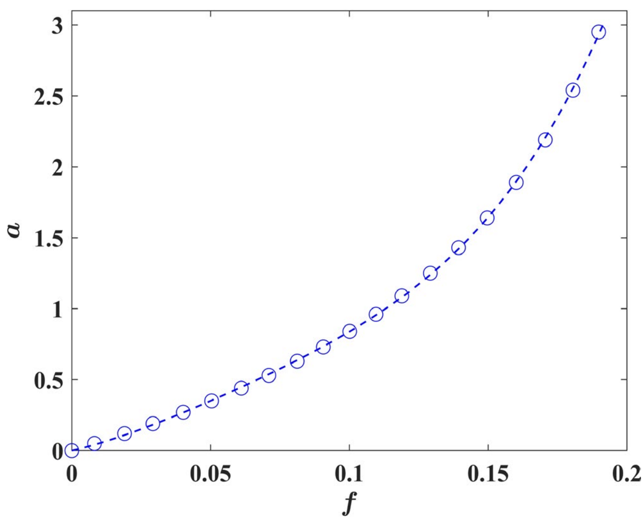

FIGURE 8 Relationship between the intercept f and volume ratio a. The scatter points represent the numerical solution of Equations (9) and (16), and the dashed line represents the approximate correlation Equation (18)

porosity ϕ can be obtained from the definition of a in Equation (4):

$$\phi = \frac{aV_u}{LA} \quad (20)$$

When θ_1 and ϕ are both known, the permeability can be easily determined with the rewritten form of Equation (17):

$$k = -\frac{\alpha\beta\mu\phi L^2}{\theta_1^2} \quad (21)$$

4 | RESULTS AND DISCUSSION

A sandstone sample was measured with the proposed method and the pressure difference was recorded to calculate the slope and intercept. During the measurements, the downstream was directly open to the atmosphere to ensure constant downstream pressure. The permeability and porosity were evaluated with slope and intercept values. To ensure the measurement repeatability and reduce random errors, the sample was measured five times, and the standard deviation of the results was found to be smaller than 5%. Table 1 shows the basic information about the sample and the measurements. Figure 10 presents one set of experimental results on pressure decay. It is noted that the experimental data shows a platform at the beginning of the test, which is consistent with the general solution in Figure 6 and the discussions in Section 3.2.1. In the semi-log plot, it can be seen that, after a short initial period, the late-time solution fits the experimental data very well and the slope and intercept values can be easily obtained through the least-squares method.

To verify the accuracy of the proposed method, the permeability and porosity measured by the proposed method were compared with those measured by the conventional pulse-decay method and the gas expansion method, and a good agreement was found, proving that the proposed method is a reliable and accurate way to estimate the permeability and porosity of tight rocks. The comparison is depicted in Table 2.

Using the slope of the pressure decay to calculate the permeability is a common characteristic shared by the pulse-decay methods. However, using the intercept to evaluate the porosity, to the authors' knowledge, has not been reported before. The common way to measure porosity is based on Boyle's law and mass conservation and requires the initial and final equilibrium pressures in the measurement. However, in the proposed method, the porosity is evaluated using late-time pressure decay data and the final equilibrium is not needed. Compared with the original pressure build-up method where the permeability and porosity are measured separately, the proposed

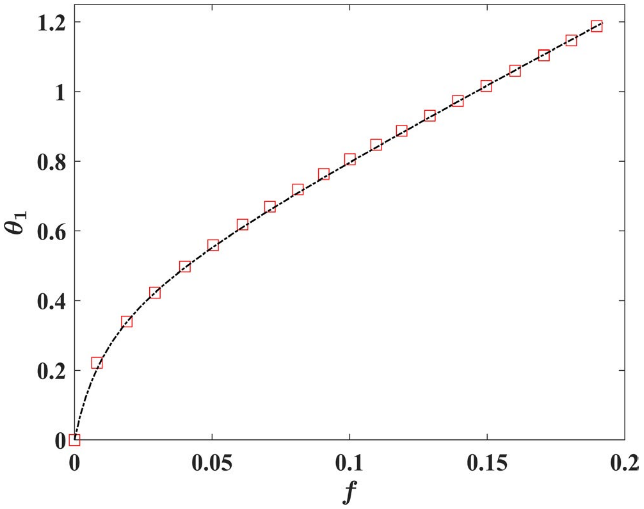

FIGURE 9 Relationship between the intercept f and θ_1. The scatter points represent the numerical solution of Equations (9) and (16), and the dashed line represents the approximate correlation Equation (19)

TABLE 1 Parameters of the measurement

Core sample	Sandstone
Testing gas	Helium
Sample length (m)	1.96×10^{-2}
Sample cross section area (m^2)	1.13×10^{-3}
Confining pressure (bar)	200
Mean pore pressure (bar)	1
Temperature (°C)	35

TABLE 2 Comparison of the measured permeability and porosity

	Permeability	Porosity
The proposed method	1.08×10^{-16} m^2	8.71%
The other method	1.06×10^{-16} m^2	8.60%
Relative error	2.14%	1.26%

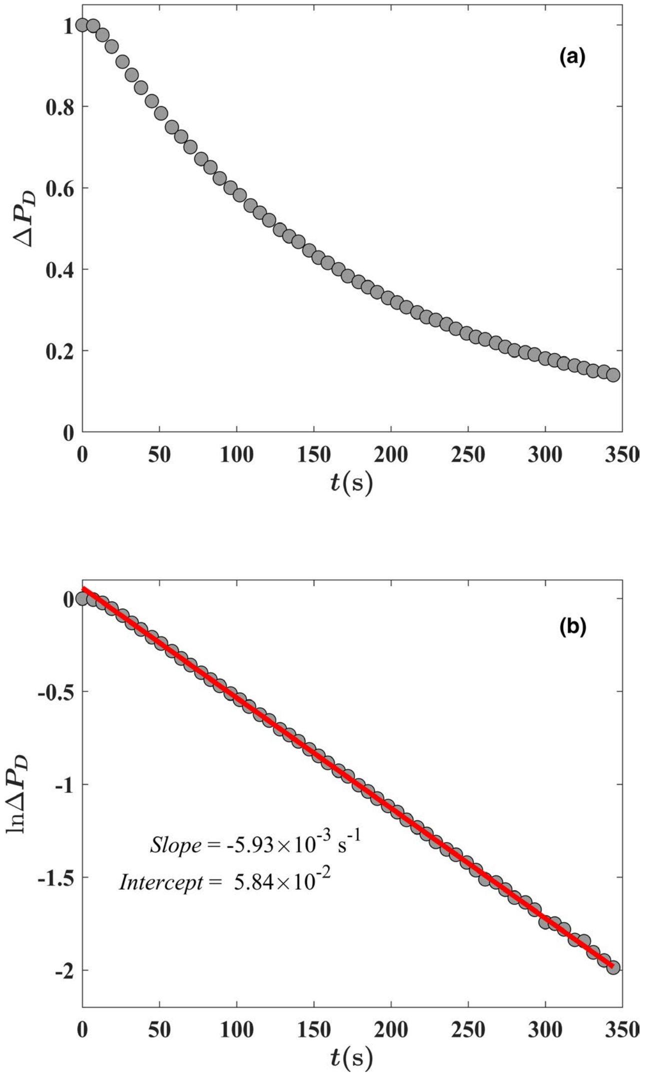

FIGURE 10 Experimental results for the sandstone sample. (A) Dimensionless pressure difference vs time. (B) Logarithmic differential pressure vs time. Note that the scatter points in (A) and (B) represent the experimental data, and the solid line in (B) represents the linear fitting curve

method has two advantages: Firstly, the total test time is significantly reduced. Secondly, the proposed method ensures the permeability and porosity are measured exactly under the same loading condition.

5 | CONCLUSIONS

In this study, a modified pressure pulse-decay method is presented to measure the permeability and porosity of a low-permeable reservoir rock. In the proposed method, the pressure on one side of the sample is changed (increased/decreased) instantaneously and then kept constant. The pressure variations on the other side are recorded to evaluate the petro-physical properties of the sample. The mathematical model describing the test process was established and the analytical solution was obtained. The late-time solution was adopted for the postprocessing of the experimental data. The permeability of the sample was determined by the slope of a semilogarithmic plot of the pressure differential vs time. A one-to-one correspondence between the volume ratio and the intercept of this plot was found, and the analytical approximate correlation of this correspondence was given. Thus, the intercept can be used to calculate the porosity of the sample. A tight sandstone sample was tested with the proposed method, and the evaluated permeability and porosity agree well with the results of the conventional methods, which confirms the accuracy of the proposed method. Compared with measuring the permeability and porosity separately, the proposed method can measure both of them in one test and under the same loading condition, which increases the accuracy and reduces the total test time.

ACKNOWLEDGMENTS

This work is financially supported by the NSFC Grant (No. U1837602, 11761131012) and the Tsinghua University Initiative Scientific Research Program. Our simulations are run on the "Explorer 100" cluster of Tsinghua National Laboratory for Information Science and Technology.

ORCID

Steffen Nolte https://orcid.org/0000-0003-2571-9719
Moran Wang https://orcid.org/0000-0002-0112-5150

REFERENCES

1. Gensterblum Y, Ghanizadeh A, Cuss RJ, et al. Gas transport and storage capacity in shale gas reservoirs–a review. Part A: transport processes. *J Unconvent Oil Gas Resour*. 2015;12:87-122.
2. Pan H, Li J, Zhang T, Li S, Zhang L. Study on crack propagation of the CO2 presplitting blasting empty hole effect in coal seam. *Energy Sci Eng*. 2020;8(11):3898-3908.
3. Soeder DJ. The successful development of gas and oil resources from shales in North America. *J Petrol Sci Eng*. 2018;163:399-420.
4. Tao S, Chen S, Pan Z. Current status, challenges, and policy suggestions for coalbed methane industry development in China: a review. *Energy Sci Eng*. 2019;7(4):1059-1074.
5. Wang Z, Wang M, Chen S. Coupling of high Knudsen number and non-ideal gas effects in microporous media. *J Fluid Mech*. 2018;840:56-73.
6. Hannon MJ. Alternative approaches for transient-flow laboratory-scale permeametry. *Transp Porous Media*. 2016;114(3):719-746.
7. Jang H, Lee W, Kim J, Lee J. Novel apparatus to measure the low-permeability and porosity in tight gas reservoir. *J Petrol Sci Eng*. 2016;142:1-12.
8. Zhao Y, Wang C, Bi J. A method for simultaneously determining axial permeability and transverse permeability of tight reservoir cores by canister degassing test. *Energy Sci Eng*. 2020;8(4):1220-1230.
9. Sander R, Pan Z, Connell LD. Laboratory measurement of low permeability unconventional gas reservoir rocks: a review of experimental methods. *J Nat Gas Sci Eng*. 2017;37:248-279.
10. Wu T, Zhang D, Li X. A radial differential pressure decay method with micro-plug samples for determining the apparent permeability of shale matrix. *J Nat Gas Sci Eng*. 2020;74:103126.
11. Akkutlu IY, Fathi E. Multiscale gas transport in shales with local kerogen heterogeneities. *SPE J*. 2012;17(04):1002-1011.
12. Heller R, Vermylen J, Zoback M. Experimental investigation of matrix permeability of gas shales. *AAPG Bull*. 2014;98(5):975-995.
13. Jones S. A technique for faster pulse-decay permeability measurements in tight rocks. *SPE Form Eval*. 1997;12(01):19-26.
14. Mokhtari M, Tutuncu AN. Characterization of anisotropy in the permeability of organic-rich shales. *J Petrol Sci Eng*. 2015;133:496-506.
15. Brace WF, Walsh J, Frangos W. Permeability of granite under high pressure. *J Geophys Res*. 1968;73(6):2225-2236.
16. Hsieh P, Tracy J, Neuzil C, Bredehoeft J, Silliman SE. A transient laboratory method for determining the hydraulic properties of 'tight'rocks—I. Theory. *Int J Rock Mech Min Sci Geomech Abstr Elsevier*. 1981;18(3):245-252.
17. Dicker A, Smits R. A practical approach for determining permeability from laboratory pressure-pulse decay measurements. In: *International Meeting on Petroleum Engineering*. Society of Petroleum Engineers. 1988:285-292.
18. Cui X, Bustin A, Bustin RM. Measurements of gas permeability and diffusivity of tight reservoir rocks: different approaches and their applications. *Geofluids*. 2009;9(3):208-223.
19. Yang Z, Dong M, Zhang S, Gong H, Li Y, Long F. A method for determining transverse permeability of tight reservoir cores by radial pressure pulse decay measurement. *J Geophysi Res: Solid Earth*. 2016;121(10):7054-7070.
20. Han G, Liu X, Huang J. Theoretical comparison of test performance of different pulse decay methods for unconventional cores. *Energies*. 2020;13(17):4557.
21. Giot R, Giraud A, Auvray C. Assessing the permeability in anisotropic and weakly permeable porous rocks using radial pulse tests. *Oil Gas Sci Technol-Revue d'IFP Energies Nouvelles*. 2014;69(7):1171-1189.
22. Cao C. Numerical interpretation of transient permeability test in tight rock. *J Rock Mech Geotech Eng*. 2018;10(1):32-41.
23. He B, Xie L, Zhao P, Ren L, Zhang Y. Highly efficient and simplified method for measuring the permeability of ultra-low permeability rocks based on the pulse-decay technique. *Rock Mech Rock Eng*. 2020;53(1):291-303.
24. Yang Z, Sang Q, Dong M, Zhang S, Li Y, Gong H. A modified pressure-pulse decay method for determining permeabilities of tight reservoir cores. *J Nat Gas Sci Eng*. 2015;27:236-246.
25. Metwally YM, Sondergeld CH. Measuring low permeabilities of gas-sands and shales using a pressure transmission technique. *Int J Rock Mech Min Sci*. 2011;48(7):1135-1144.
26. Wang Y, Chen Z, Morah V, Knabe R, Appel M. Gas-phase relative permeability characterization on tight-gas samples. *Petrophysics*. 2012;53(06):393-400.
27. Li Z, Feng R, Liu J, Pandey R. A simplified transient technique for porosity and permeability determination in tight formations: numerical simulation and experimental validation. *Energy Sci Eng*. 2021;9(3):375-389.
28. Wang C, Pan L, Zhao Y, Zhang Y, Shen W. Analysis of the pressure-pulse propagation in rock: a new approach to simultaneously determine permeability, porosity, and adsorption capacity. *Rock Mech Rock Eng*. 2019;52(11):4301-4317.
29. Gaus G, Amann-Hildenbrand A, Krooss BM, Fink R. Gas permeability tests on core plugs from unconventional reservoir rocks under controlled stress: a comparison of different transient methods. *J Nat Gas Sci Eng*. 2019;65:224-236.
30. Nolte S, Fink R, Krooss BM, et al. Experimental investigation of gas dynamic effects using nanoporous synthetic materials as tight rock analogues. *Transp Porous Media*. 2021;137(3):519-553.
31. Fink R, Krooss B, Amann-Hildenbrand A. Stress-dependence of porosity and permeability of the Upper Jurassic Bossier shale: an experimental study. *Geol Soc, Lond, Spec Publ*. 2017;454(1):107-130.
32. Song W, Yao J, Li Y, et al. Apparent gas permeability in an organic-rich shale reservoir. *Fuel*. 2016;181:973-984.

33. Zhao Y, Wang C, Bi J. Permeability model of fractured rock with consideration of elastic-plastic deformation. *Energy Sci Eng*. 2020;8(2):441-451.
34. Walder J, Nur A. Permeability measurement by the pulse-decay method: effects of poroelastic phenomena and non-linear pore pressure diffusion. *Int J Rock Mech Min Sci Geomech Abstr*. 1986;23(3):225-232.
35. Winhausen L, Amann-Hildenbrand A, Fink R, et al. A comparative study on methods for determining the hydraulic properties of a clay shale. *Geophys J Int*. 2021;224(3):1523-1539.
36. Zheng J, Zheng L, Liu H-H, Ju Y. Relationships between permeability, porosity and effective stress for low-permeability sedimentary rock. *Int J Rock Mech Min Sci*. 2015;78:304-318.
37. Hahn DW, Özisik MN. *Heat Conduction*. John Wiley & Sons; 2012.

How to cite this article: Wang Y, Nolte S, Tian Z, Amann-Hildenbrand A, Krooss B, Wang M. A modified pulse-decay approach to simultaneously measure permeability and porosity of tight rocks. *Energy Sci Eng*. 2021;00:1–10. doi:10.1002/ese3.989

APPENDIX A

The procedure for solving Equations (5)-(7) through the Laplace transform is presented in this appendix.

The Laplace transform of the dimensionless pressure $P_D(x_D, t_D)$ is defined as:

$$\overline{P}_D(x_D, s) = \mathscr{L}\left[P_D(x_D, t_D)\right] = \int_0^{+\infty} P_D(x_D, t_D)\, e^{-st_D} dt_D \quad \text{(A1)}$$

where $\overline{P}_D$ is the transformed counterpart of P_D and s is the transform parameter.

Applying the Laplace transform to the Equations (5)-(7), we obtain the transformed governing equation:

$$\frac{d\overline{P}_D(x_D, s)}{dx_D} = s\overline{P}_D(x_D, s) - 1 \quad \text{(A2)}$$

and the transformed boundary conditions:

$$s\overline{P}_D(0, s) - P_D(0, 0) = a\left.\frac{d\overline{P}_D}{dx_D}\right|_{x_D=0}, \quad \overline{P}_D(1, s) = 0 \quad \text{(A3)}$$

Note that the initial conditions have been substituted into the above transformed equations.

Combining the transformed Equations (A2) and (A3), we get the expression for $\overline{P}_D(x_D, s)$:

$$\overline{P}_D(x_D, s) = \frac{1}{s} - \frac{\sqrt{s}\sinh\left(\sqrt{s}x_D\right) + a\cosh\left(\sqrt{s}x_D\right)}{s\left[\sqrt{s}\sinh\left(\sqrt{s}\right) + a\cosh\left(\sqrt{s}\right)\right]} \quad \text{(A4)}$$

Then $P_D(x_D, t_D)$ can be obtained by applying the inverse Laplace transform to $\overline{P}_D(x_D, s)$:

$$P_D(x_D, t_D) = \mathscr{L}^{-1}\left[\overline{P}_D(x_D, s)\right] = \frac{1}{2\pi i}\int_{c-i\infty}^{c+i\infty} e^{st_D}\overline{P}_D(x_D, s)\, ds \quad \text{(A5)}$$

where s is now a complex number, and c is a real, positive constant that is large enough that all the singularities of $\overline{P}_D(x_D, s)$ lie to the left of the line $(c - i\infty, c + i\infty)$.

The contour integral in Equation (A5) can be evaluated through Cauchy's residue theorem:

$$\overline{P}_D(x_D, t_D) = m\sum \text{Res}\left[e^{st_D}\overline{P}_D(x_D, s), s_m\right] \quad \text{(A6)}$$

where s_m are the poles of the integrand $e^{st_D}\overline{P}_D(x_D, s)$, and $\text{Res}\left[e^{st_D}\overline{P}_D(x_D, s), s_m\right]$ are the corresponding residues.

To determine the poles of $e^{st_D}\overline{P}_D(x_D, s)$, we set $\sqrt{s_m} = i\theta_m$ and substitute it into the denominator of $\overline{P}_D(x_D, s)$:

$$\theta_m^3\sin\theta_m - a\theta_m^2\cos\theta_m = 0 \quad \text{(A7)}$$

It is easy to check that $\theta_0 = 0$ satisfies Equation (A7), and $\theta_m\,(m \geq 1)$ are the roots of the following equation:

$$\tan\theta_m = \frac{a}{\theta_m} \quad (m \geq 1) \quad \text{(A8)}$$

Since Equation (A8) has infinite real roots and all of them are of the first order, the integrand has infinite real, nonpositive simple poles (recalling that $\sqrt{s_m} = i\theta_m$):

$$s_0 = 0, s_m = -\theta_m^2 \quad (m \geq 1) \quad \text{(A9)}$$

Noting that if $\theta_m\,(m \geq 1)$ is the root of Equation (A8), so will be $-\theta_m$, and the sign of θ_m has no effect on the value of s_m. Therefore, we take $\theta_m\,(m \geq 1)$ to be positive in the following derivation, without a loss of generality.

Then, we evaluate the residue of the pole $s_0 = 0$:

$$\mathrm{Res}\left[e^{st_D}\overline{P}_D\left(x_D,s\right),0\right] = \lim_{s\to 0}\left[se^{st_D}\overline{P}_D\left(x_D,s\right)\right] = 0 \tag{A10}$$

and the residues of the other poles $s_m = -\theta_m^2\ (m \geq 1)$ are as follows:

$$\mathrm{Res}\left[e^{st_D}\overline{P}_D\left(x_D,s\right), -\theta_m^2\right] = \lim_{s\to -\theta_m^2}\left[\left(s+\theta_m^2\right)e^{st_D}\overline{P}_D\left(x_D,s\right)\right] = 2\frac{a\cos\left(\theta_m x_D\right) - \theta_m \sin\left(\theta_m x_D\right)}{\left(\theta_m^2 + a^2 + a\right)\cos\theta_m}e^{-\theta_m^2 t_D} \tag{A11}$$

Substituting Equations (A10) and (A11) into Equation (A6), we get the expression for $P_D\left(x_D, t_D\right)$:

$$P_D\left(x_D, t_D\right) = 2\sum_{m=1}^{\infty}\frac{a\cos\left(\theta_m x_D\right) - \theta_m \sin\left(\theta_m x_D\right)}{\left(\theta_m^2 + a^2 + a\right)\cos\left(\theta_m\right)}e^{-\theta_m^2 t_D} \tag{A12}$$

where $\theta_m\ (m \geq 1)$ are the positive roots of Equation (A8).

APPENDIX B

In addition to the exact series solution derived in Appendix A, Laplace transform can also help to derive the approximate solution applicable for very small values of time. Since the downstream pressure is kept constant during the test, we focus on the upstream pressure variations within a short period of time after the start of the test.

By letting $x_D = 0$ in Equation (A4), the expression for the transformed upstream pressure $\overline{P}_{uD}(s)$ can be obtained:

$$\overline{P}_{uD}(s) = \overline{P}_D(0,s) = \frac{1}{s} - \frac{2a}{s\left(\sqrt{s}+a\right)e^{\sqrt{s}} - s\left(\sqrt{s}-a\right)e^{-\sqrt{s}}} = \frac{1}{s} - \frac{2a}{s\left(\sqrt{s}+a\right)e^{\sqrt{s}}}\left(1 - \frac{\sqrt{s}-a}{\sqrt{s}+a}e^{-2\sqrt{s}}\right)^{-1} \tag{B1}$$

where the hyperbolics have been converted into exponentials.

The last term in Equation (B1) can be expanded as a Taylor series:

$$\left(1 - \frac{\sqrt{s}-a}{\sqrt{s}+a}e^{-2\sqrt{s}}\right)^{-1} = 1 + \left(\frac{\sqrt{s}-a}{\sqrt{s}+a}e^{-2\sqrt{s}}\right)^1 + \left(\frac{\sqrt{s}-a}{\sqrt{s}+a}e^{-2\sqrt{s}}\right)^2 + \cdots \tag{B2}$$

and thus Equation (B1) can be rewritten as:

$$\overline{P}_{uD}(s) = \frac{1}{s} - \frac{2a}{s\left(\sqrt{s}+a\right)e^{\sqrt{s}}}\left[1 + \left(\frac{\sqrt{s}-a}{\sqrt{s}+a}e^{-2\sqrt{s}}\right)^1 + \left(\frac{\sqrt{s}-a}{\sqrt{s}+a}e^{-2\sqrt{s}}\right)^2 + \cdots\right] \tag{B3}$$

By applying the inverse Laplace transform to each term on the right-hand side of Equation (B3), the exact expression for $P_{uD}\left(t_D\right)$ can be obtained, which should also be in the form of a series. The inverse Laplace transform of the first two terms in Equation (B3) can be found from the published Laplace transform tables[37]:

$$\mathscr{L}^{-1}\left[\frac{1}{s}\right] = 1 \tag{B4}$$

$$\mathscr{L}^{-1}\left[-\frac{2a}{s\left(\sqrt{s}+a\right)e^{\sqrt{s}}}\right] = 2e^{a+a^2t_D}\mathrm{erfc}\left(a\sqrt{t_D} + \frac{1}{2\sqrt{t_D}}\right) - 2\mathrm{erfc}\left(\frac{1}{2\sqrt{t_D}}\right) \tag{B5}$$

and those of the remaining terms involve very complex expressions and cannot be written down in a concise manner. However, it can be proved that the inverse Laplace transform of the remaining terms is much smaller than that of the first two terms when the dimensionless time t_D is small. Therefore, by retaining the first few terms of the inverted series, an approximate expression of upstream pressure variations in a short time can be obtained:

$$P_{uD}\left(t_D\right) \approx 1 + 2e^{a+a^2t_D}\mathrm{erfc}\left(a\sqrt{t_D} + \frac{1}{2\sqrt{t_D}}\right) - 2\mathrm{erfc}\left(\frac{1}{2\sqrt{t_D}}\right) \tag{B6}$$